Expanded View Figures

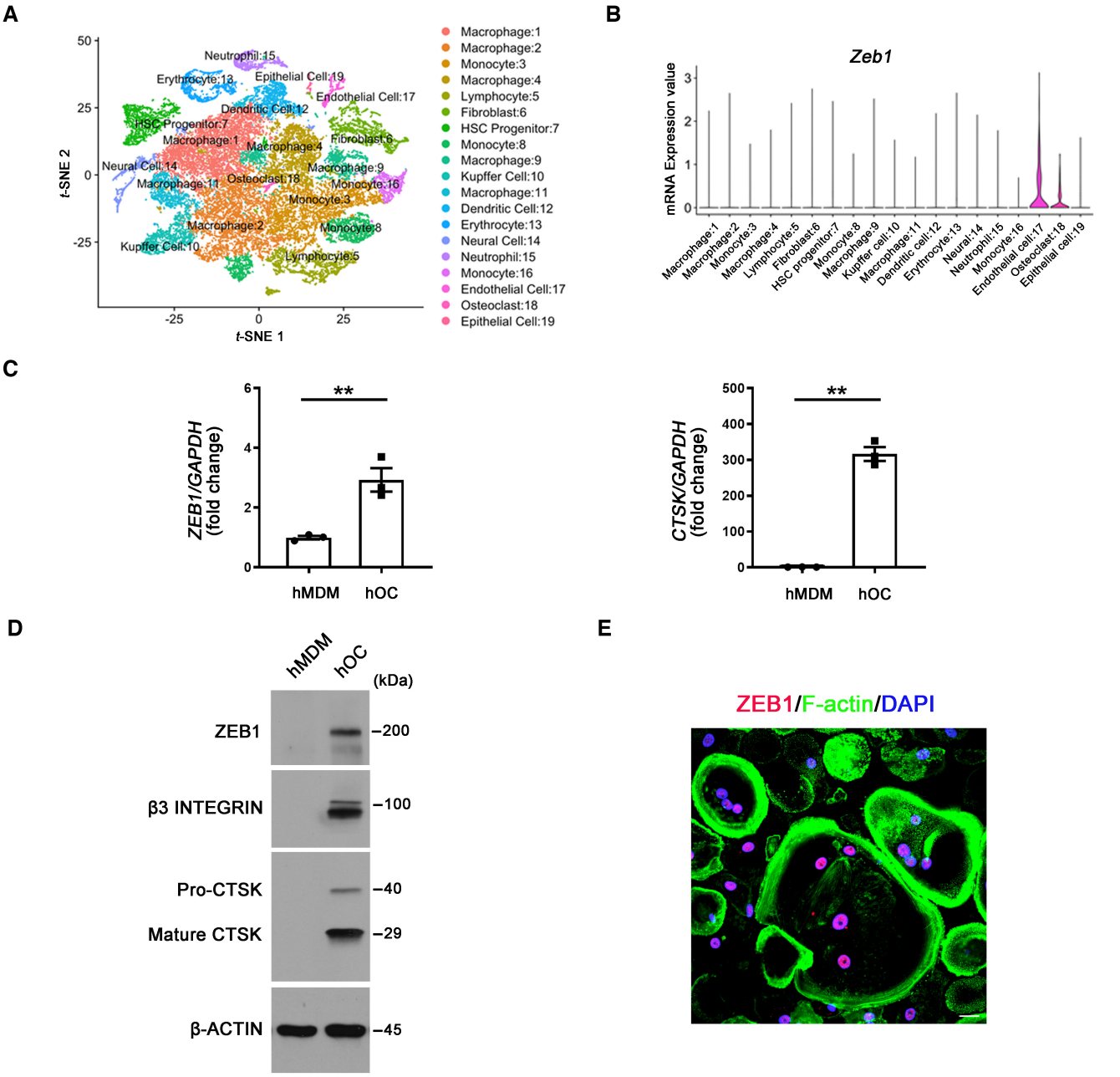

Figure EV1. Osteoclasts upregulate Zeb1 mouse and human osteoclasts.

A *t*-Distributed stochastic neighbor embedding (*t*-SNE) plots of cells from E14.5 embryos identified 19 clusters including osteoclasts (Data ref: Yahara *et al*, 2020b).

B Violin plots showing mRNA expression value of *Zeb1* in each cell cluster from E14.5 embryos *in vivo*, with the x axis number representing cluster identity (Data ref: Yahara *et al*, 2020b).

C Relative mRNA expression of *ZEB1* and *CTSK* in human monocyte-derived macrophages (hMDMs) and mature human osteoclasts (hOC; $n = 3$).

D ZEB1, β3 INTEGRIN, and CTSK protein expression as assessed by Western blot were determined in hMDMs and mature hOCs.

E ZEB1 (red) and F-actin (green) staining of human osteoclasts differentiated from hMDM. Scale bar, 20 μm.

Data information: Bars and error bars represent mean ± SEM. Data are representative of at least three independent experiments with biological replicates. Data were analyzed using unpaired Student's *t* test (C). $^{**}P < 0.01$.
Source data are available online for this figure.

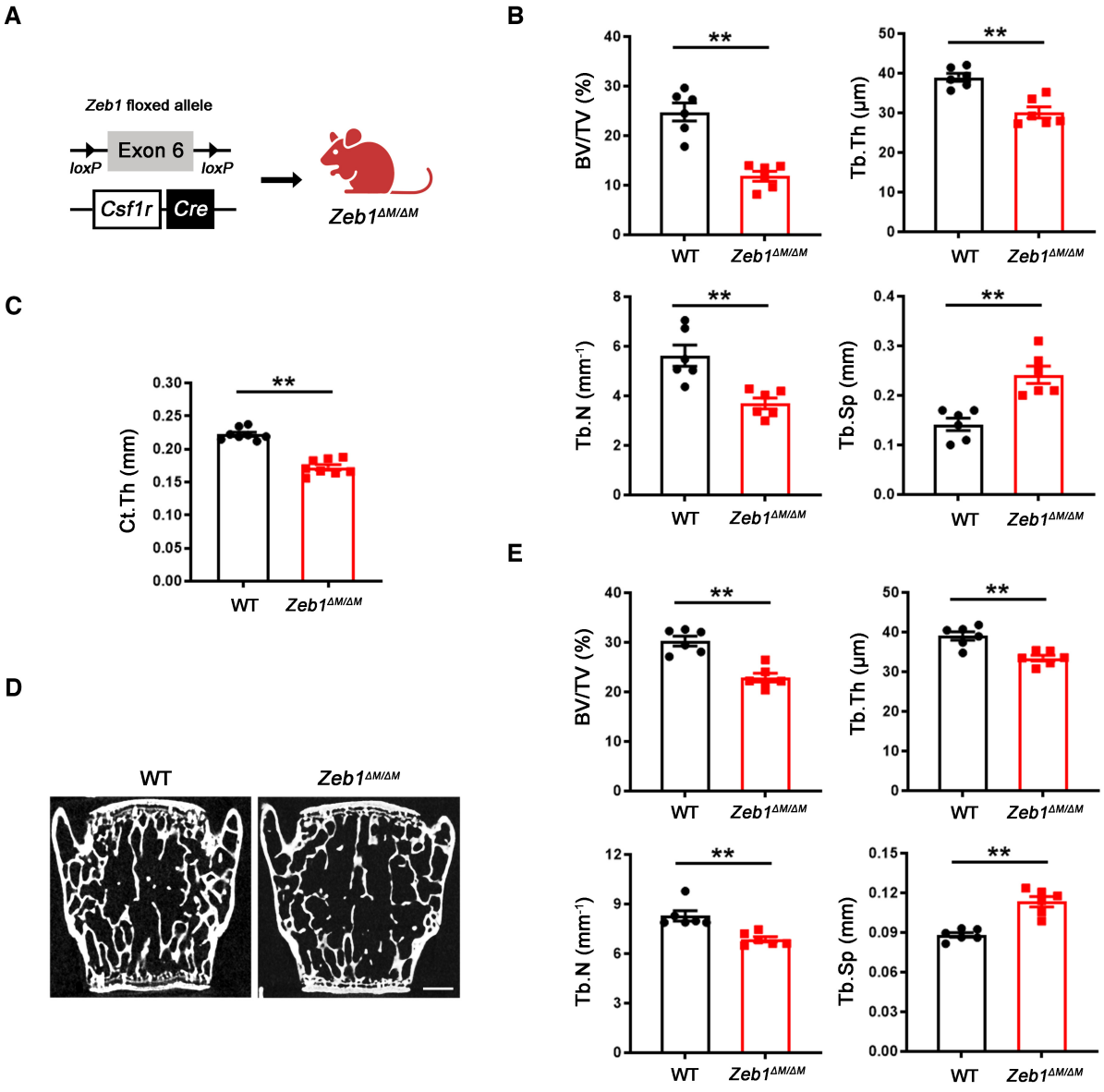

Figure EV2. *Zeb1*$^{\Delta M/\Delta M}$ mice exhibit decreased bone mass in femur and lumbar vertebrae.

A Schematic of breeding strategy to generate myeloid-selective *Zeb1* knockout mice (*Csf1r- Cre/Zeb1*$^{f/f}$; *Zeb1*$^{\Delta M/\Delta}$).

B Quantification of BV/TV, Tb.Th, Tb.N, and Tb.Sp as determined by nanoCT in 3-month-old wild-type and *Zeb1*$^{\Delta M/\Delta M}$ female mice (n = 6).

C Quantification of cortical thickness (Ct.Th) as determined by nanoCT in femurs of 3 month-old wild-type and *Zeb1*$^{\Delta M/\Delta M}$ male mice (n = 8).

D Representative nanoCT of L3 vertebrae sections of 3-month-old wild-type and *Zeb1*$^{\Delta M/\Delta M}$ male mice are shown. Scale bar, 500 μm.

E Quantification of BV/TV, Tb.Th, Tb.N, and Tb.Sp as determined by nanoCT in L3 vertebrae of 3 month-old wild-type and *Zeb1*$^{\Delta M/\Delta M}$ male mice (n = 6). $^{**}P < 0.01$.

Data information: Bars and error bars represent mean ± SEM. Data are representative of at least three independent experiments with biological replicates. Data were analyzed using unpaired Student's t test (B, C, E). $^{**}P < 0.01$.

Figure EV3. Zeb1 negatively regulates MtCK1 expression in mouse and human osteoclasts.

A Relative expression of creatine metabolism-related transcripts during wild-type BMDM-osteoclast transition as retrieved from gene profiling data set (Zhu *et al*, 2020).

B Relative mRNA expression of *Slc6a8*, *Slc6a12*, *Gatm*, *Gamt*, *MtCK2*, *Ckb*, and *Ckm* in BMDMs and osteoclasts generated from wild-type or $Zeb1^{\Delta M/\Delta M}$ mice (n = 3).

C An empty control vector (EV)-transduced wild-type BMDMs and EV- or ZEB1-transduced $Zeb1^{\Delta M/\Delta M}$ BMDMs were differentiated into osteoclasts and cell lysates collected for MtCK1, Ckb, VDAC, c-Src, and Ctsk immunoblotting (n = 3).

D MtCK1 (green) and TRAP (red) immunofluorescence of a femur section from wild-type and $Zeb1^{\Delta M/\Delta M}$ mice. GP, growth plate. Scale bar, 20 μm.

E, F hMDMs were transfected with either a nontargeting control siRNA (si*CTRL*) or siRNA targeting *ZEB1*, differentiated into osteoclasts, and cell lysates collected for ZEB1, MtCK1, CKB, c-SRC, and CTSK immunoblotting (E) and quantified (F; n = 3).

G, H MtCK1 (red) immunofluorescence of si*CTRL*- or *siZEB1-transfected* human osteoclasts (H) and quantified (G; n = 3). Scale bar, 20 μm.

Data information: Bars and error bars represent mean ± SEM. Data are representative of at least three independent experiments with biological replicates. Data were analyzed using two-way ANOVA with Bonferroni correction (B) and one-way ANOVA with Bonferroni correction (F, G). ns, not significant; $*P < 0.05$, $**P < 0.01$.
Source data are available online for this figure.

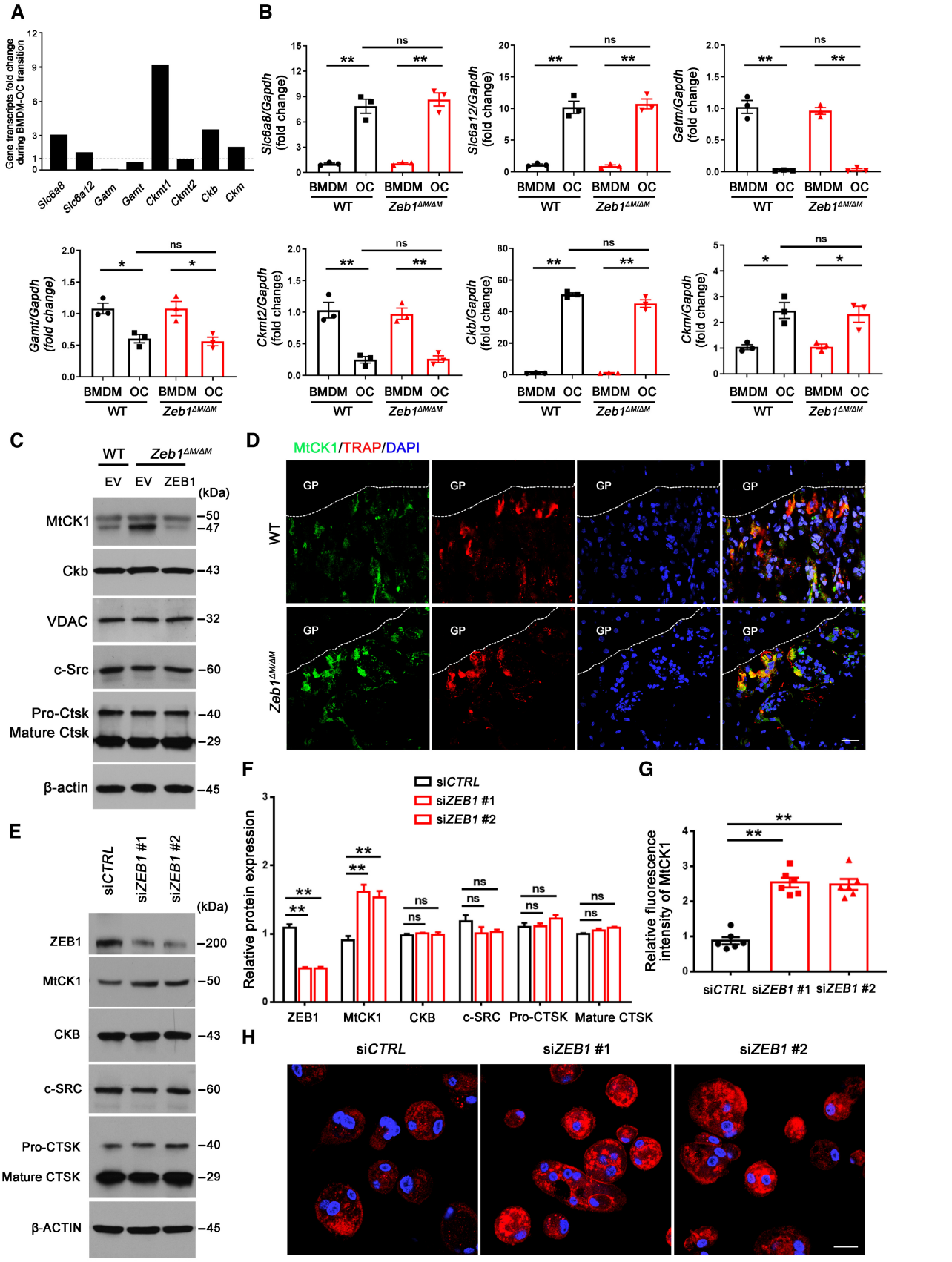
A
Gene transcripts fold change during BMDM-OC transition
Slc6a8
Slc6a12
Gatm
Gamt
Ckmt1
Ckmt2
Ckb
Ckm
B
Slc6a8/Gapdh (fold change)
Slc6a12/Gapdh (fold change)
Gatm/Gapdh (fold change)
Gamt/Gapdh (fold change)
Ckmt2/Gapdh (fold change)
Ckb/Gapdh (fold change)
Ckm/Gapdh (fold change)
BMDM OC BMDM OC
WT Zeb1ΔM/ΔM
ns
C
WT Zeb1ΔM/ΔM
EV EV ZEB1
(kDa)
MtCK1
Ckb
VDAC
c-Src
Pro-Ctsk
Mature Ctsk
β-actin
D
MtCK1/TRAP/DAPI
WT
Zeb1ΔM/ΔM
GP
E
siCTRL
siZEB1 #1
siZEB1 #2
(kDa)
ZEB1
MtCK1
CKB
c-SRC
Pro-CTSK
Mature CTSK
β-ACTIN
F
siCTRL
siZEB1 #1
siZEB1 #2
Relative protein expression
ZEB1 MtCK1 CKB c-SRC Pro-CTSK Mature CTSK
G
Relative fluorescence intensity of MtCK1
siCTRL siZEB1 #1 siZEB1 #2
H
siCTRL
siZEB1 #1
siZEB1 #2

Figure EV3.

Figure EV4. Zeb1-dependent mitochondrial creatine kinase activity drives osteoclast activation.

A Wild-type osteoclasts were cultured with exogenous 2 μM phosphocreatine and RhoA activity determined (n = 6).

B–D TRAP (red), WGA-DAB and phalloidin staining (red) of wild-type osteoclasts cultured atop bone slices in the presence of exogenous 2 μM phosphocreatine (D). Scale bar, upper and middle 100 μm, lower 20 μm. The number of $TRAP^+$ MNCs, resorption pit area, and actin ring area per cell were quantified (B and C; n = 6).

E Scrambled shRNA control vector (sh*Ctrl*)-transduced wild-type BMDMs, and sh*Ctrl*- or sh*Ckmt1*-transduced $Zeb1^{\Delta M/\Delta M}$ BMDMs, were differentiated into osteoclasts, and cell lysates collected for MtCK1, Ckb, Tomm20, VDAC, Zeb1, c-Src, and Ctsk immunoblotting (n = 3).

F Mitochondrial creatine kinase activity of sh*Ctrl*-transduced wild-type osteoclasts, and sh*Ctrl*- or sh*Ckmt1*-transduced $Zeb1^{\Delta M/\Delta M}$ osteoclasts cultured on plastic (n = 3).

G PCr/Cr ratio of scrambled sh*Ctrl*-transduced wild-type osteoclasts, and sh*Ctrl*- or sh*Ckmt1*-transduced $Zeb1^{\Delta M/\Delta M}$ osteoclasts cultured on plastic as determined by LC/MS analysis (n = 3).

H, I ATP levels (H) and RhoA activity (I) of sh*Ctrl*-transduced wild-type osteoclasts, and sh*Ctrl*- or sh*Ckmt1*-transduced $Zeb1^{\Delta M/\Delta M}$ osteoclasts (n = 3).

J, K sh*Ctrl*-transduced wild-type preosteoclasts, and sh*Ctrl*- or sh*Ckmt1*-transduced $Zeb1^{\Delta M/\Delta M}$ pre-osteoclasts were cultured atop bone slices for 3 days, stained with phalloidin (red). Osteoclasts were removed and resorption pits visualized by WGA-DAB staining (K). Scale bar, upper 20 μm, lower 100 μm. The actin ring area per cell and resorption pit area were quantified (J).

Data information: Bars and error bars represent mean ± SEM. Data are representative of at least three independent experiments with biological replicates. Data were analyzed using unpaired Student's t test (A–C) or one-way ANOVA with Bonferroni correction (F–J). ns, not significant; $^{**}P < 0.01$.
Source data are available online for this figure.

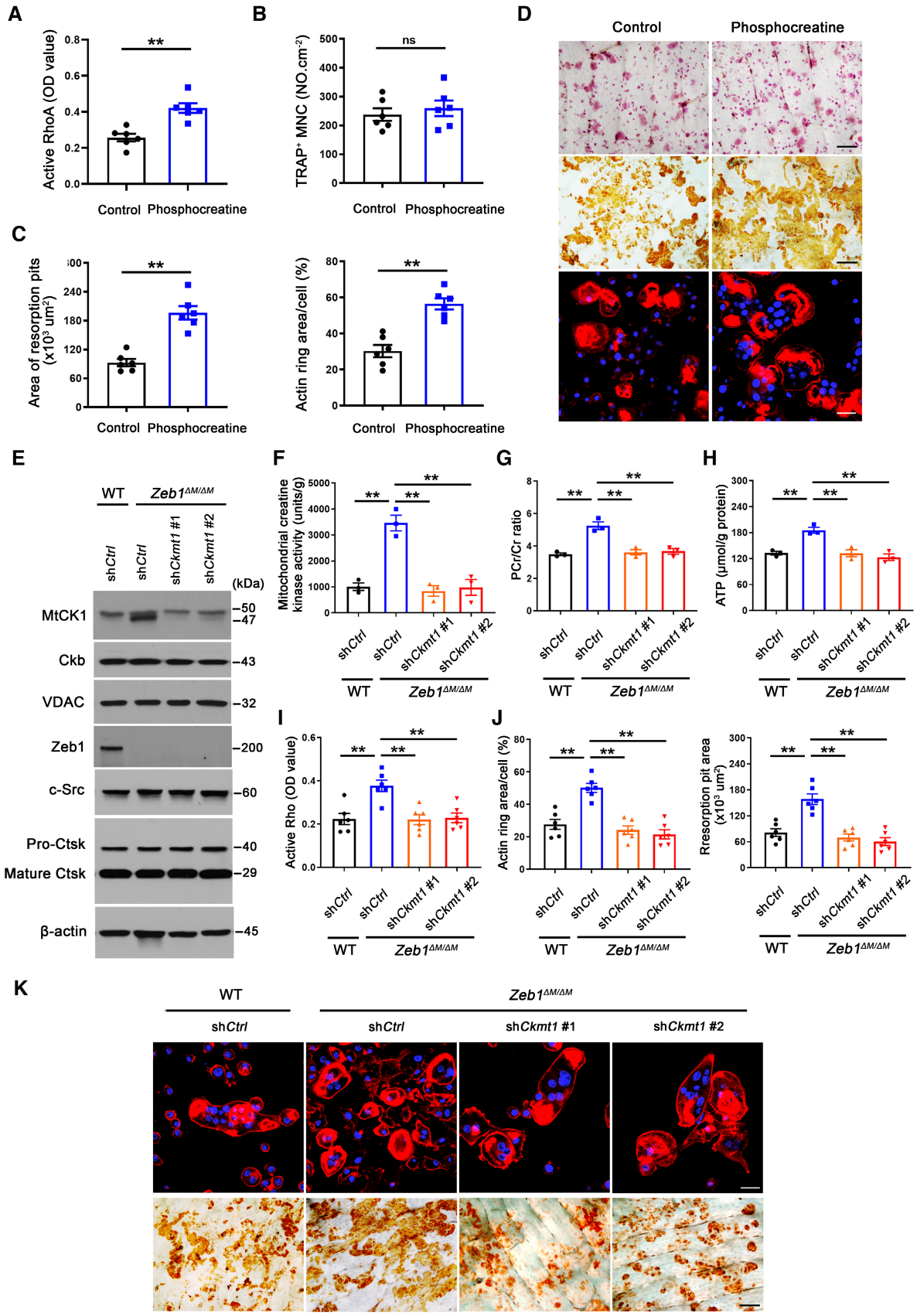
A
Active RhoA (OD value)
Control Phosphocreatine
B
TRAP+ MNC (NO.cm-2)
ns
Control Phosphocreatine
C
Area of resorption pits (x10³ um²)
Actin ring area/cell (%)
Control Phosphocreatine
D
Control
Phosphocreatine
E
WT
Zeb1ΔM/ΔM
shCtrl
shCtrl
shCkmt1 #1
shCkmt1 #2
(kDa)
MtCK1
Ckb
VDAC
Zeb1
c-Src
Pro-Ctsk
Mature Ctsk
β-actin
F
Mitochondrial creatine kinase activity (units/g)
G
PCr/Cr ratio
H
ATP (μmol/g protein)
I
Active Rho (OD value)
J
Actin ring area/cell (%)
Resorption pit area (x10³ um²)
K
WT
Zeb1ΔM/ΔM
shCtrl
shCtrl
shCkmt1 #1
shCkmt1 #2

Figure EV4.

Figure EV5. MtCK1 regulates human osteoclast mitochondrial bioenergetics and bone resorption.

A hMDMs were transfected with either nontargeting si*CTRL* or siRNA targeting *CKMT1*, differentiated into osteoclasts, and cell lysates collected for MtCK1, CKB, ZEB1, c-SRC, and CTSK immunoblotting ($n = 3$).

B Mitochondrial creatine kinase activity of si*CTRL*- or si*CKMT1*-transfected osteoclasts cultured on plastic ($n = 3$).

C Phosphocreatine/creatine (PCr/Cr) ratio of si*CTRL*- or si*CKMT1*-transfected osteoclasts cultured on plastic as determined by LC/MS analysis ($n = 3$).

D, E ATP levels (D) and RhoA activity (E) of si*CTRL*- or si*CKMT1*-transfected osteoclasts.

F Mitochondrial function parameters analyzed by XF Cell Mito Stress Assay in si*CTRL*- or si*CKMT1*-transfected osteoclasts after sequential treatment of compounds modulating mitochondrial function ($n = 4$).

G, H si*CTRL*- or si*CKMT1*-transfected human osteoclasts were cultured atop bone slices for 3 days, stained with phalloidin (red). Osteoclasts were removed and resorption pits visualized by WGA-DAB staining (G). Scale bar, upper 20 μm, middle and lower 100 μm. The actin ring area per cell and resorption pit area were quantified (H; $n = 6$).

I TRAP, resorption pits visualized with WGA-DAB staining, and phalloidin staining in wild-type osteoclasts treated with vehicle, and $Zeb1^{\Delta M/\Delta M}$ osteoclasts treated with vehicle or 200 μM cyclocreatine cultured on bone slices with the number of $TRAP^+$ MNCs, resorption pit area, and actin ring area per cell quantified ($n = 6$).

Data information: Bars and error bars represent mean ± SEM. Data are representative of at least three independent experiments with biological replicates. Data were analyzed using one-way ANOVA with Bonferroni correction (B–F, H, I). ns, not significant; $*P < 0.05$, $**P < 0.01$.
Source data are available online for this figure.

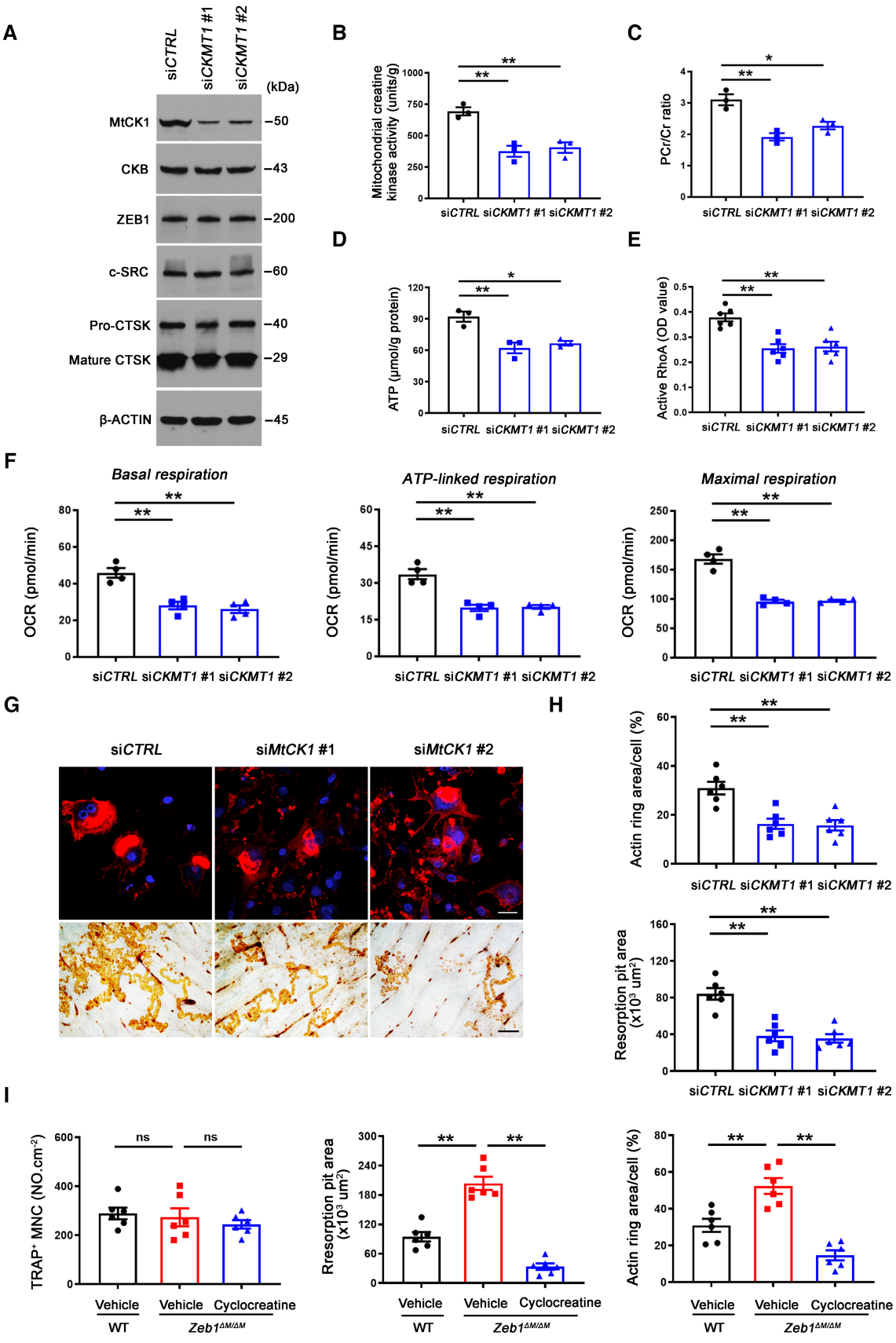
A
siCTRL
siCKMT1 #1
siCKMT1 #2
(kDa)
MtCK1
CKB
ZEB1
c-SRC
Pro-CTSK
Mature CTSK
β-ACTIN
–50
–43
–200
–60
–40
–29
–45
B
Mitochondrial creatine kinase activity (units/g)
C
PCr/Cr ratio
D
ATP (μmol/g protein)
E
Active RhoA (OD value)
F
Basal respiration
ATP-linked respiration
Maximal respiration
OCR (pmol/min)
G
siCTRL
siMtCK1 #1
siMtCK1 #2
H
Actin ring area/cell (%)
Resorption pit area (x10³ um²)
I
TRAP⁺ MNC (NO.cm⁻²)
Rresorption pit area (x10³ um²)
Actin ring area/cell (%)
ns
Vehicle
Cyclocreatine
WT
Zeb1ΔM/ΔM

Figure EV5.